



**EFFECT OF SILVER ADDITION ON THE STRUCTURE AND
METHYLENE BLUE PHOTODAGRADATION CAPACITY OF
TITANIA SYNTHESISED VIA A SURFACTANT TEMPLATE ROUTE**

Carolina E. Zubieta^{1,2}, Paula V. Messina^{1,2}, Marisa Frechero^{1,2} and Pablo C. Schulz^{1♥}

¹*Departamento de Química e INQUISUR, Universidad Nacional del Sur, Bahía Blanca, Argentina.*

²*CONICET, Argentina.*

Received March 1, 2009. In final form August 3, 2010.

Abstract

Mesoporous titania was synthesized by a surfactant template route and was doped with Ag₂O by treatment with AgNO₃. Commercial anatase was also used as reference material. The obtained materials were characterized by nitrogen adsorption, scanning and transmission electron microscopy, solid state conductivity and X-ray diffraction. The inclusion of Ag reduced the specific area of the mesoporous

♥Corresponding author. E mail: pschulz@criba.edu.ar Tel +54(291)4548305 Fax: + 54 (291) 4595160

material, modified its composition and aggregation state and produced heterogeneous surface depending on the Ag content. The conductivity of the solids is increased by Ag inclusion, but the increased activation energy reflects the difficulty of moving the larger Ag^+ ions in comparison with Ti^{4+} ones. Methylene blue was used as a reactive testing dye. The adsorption followed a first order kinetics. The thermodynamics of adsorption was studied. The photodegradation was studied by UV irradiation. The Ag-treated materials had better photodegradative behavior than the original non-doped one.

Keywords: silver doped titania; methylene blue; photodegradation; adsorption; pollution

Resumen

Se sintetizó óxido de titanio a través de una ruta de plantilla de surfactante, y fue dopado con Ag_2O mediante un tratamiento con AgNO_3 . Se usó como referencia anatasa comercial. Los materiales obtenidos fueron caracterizados mediante adsorción de nitrógeno, microscopía electrónica de transmisión y de barrido, conductividad del estado sólido y difracción de rayos X. La inclusión de plata redujo el área específica del material mesoporoso, modificó su composición y su estado de agregación y produjo una superficie heterogénea que dependió del contenido de plata. La conductividad del sólido aumentó con la inclusión de plata, pero el aumento de la energía de activación reflejó la mayor dificultad para mover los iones Ag^+ de mayor tamaño que los Ti^{4+} . Como colorante reactivo de ensayo se usó azul de metileno. Su adsorción siguió una cinética de primer orden. Se estudió además su termodinámica de adsorción. La fotodegradación del colorante se estudió por irradiación UV. Los materiales tratados con plata mostraron mejor comportamiento fotodegradativo que el material original no tratado.

Palabras clave: titanio dopado con plata; azul de metileno; fotodegradación; adsorción; polución

Introduction

Reactive dyes are the largest single group of dyes used in textile industry. Being highly water soluble they produce serious problems in environment. Nearly 50 % of reactive dyes may be lost to the effluent during dyeing process of cellulose fibers. It is estimated that 400 tons daily find their way into the environment, primary dissolved or suspended in water. Such colored waste produces disturbs in biological process because some of them are toxic for aquatic organisms and reduce the oxygen present in water.

Titanium dioxide has been widely used due to their advantages: it is non toxic, inexpensive, has high photocatalytic activity and efficiency to degrade organic materials in a process that only consumes atmospheric oxygen. TiO_2 has three crystalline phases: anatase, brookite and rutile, being anatase the material that shows the highest photocatalytic activity, which is attributable to the low recombination rate of its photo-generated electrons and holes [1]. However, for practical applications, the photocatalytic activity of TiO_2 needs further improvement. For this reason, much attention has been paid to doping the material with transition and noble metals, such as Pd [2], Pt [3,4], Rh [3], Au [5] and Ag [6,7]. Ag is the most promising one for the improvement of the photocatalytic activity of TiO_2 [7]. Ag increases the electron hole separation and can also facilitate the electron excitation by creating a local electric field. [8].

The materials' properties like photodegradation capacity and adsorption depend strongly on the procedure of preparation.[9].

The goal of this work is to evaluate the capacity for elimination of reactive dyes from aqueous solutions and the degradation power by the utilization of TiO_2 mesoporous materials synthesized via surfactant templates and doped with Ag, to determine if there is an improvement in photocatalytic activity compared to pure commercial TiO_2 (99% anatase from Aldrich) and a pure titania material prepared from Ti (IV) isopropoxide. The dye employed to study this capacity was methylene blue (MB).

The materials were characterized using X-ray powder diffraction (XRD), Scanning Electron Microscopy (SEM), Transmission Electron Microscopy (TEM), Nitrogen adsorption isotherms and Solid State Conductivity (SSC).

Experimental

Materials and methods

Synthesis

The synthesis of TiO₂ materials was performed by a surfactant template route as follows: 11.6 mL of Ti (IV) isopropoxide (Analyticals Carlo Erba 98%) was mixed with 2 mL double distilled water and stirred by 2 min at 500 rpm. Then a solution of 7.65 g of hexadecyltrimethylammonium bromide (HTAB, also known as cetyltrimethylammonium bromide, CTAB, Aldrich 99%) in 38 mL water was added. The resulting gel was stirred by 3 min and left 48 h in hydrothermal treatment at 100 °C in autoclave. The obtained gel was filtered, washed several times with double distilled water and left to dry at room temperature. Then it was calcinated for 7 h at 540 °C under air flux. This material is referred as the as-synthesized titania (AST)

Then part of the AST was immersed in a 0.01 M solution of AgNO₃ (analytical grade from Merck 99%), and another part in 0.05 M solution of AgNO₃ and left for 24 hours. Next the material was filtered and left to dry at room temperature. We obtained two materials with different Ag content: 3.4 mg Ag₂O/g TiO₂ (referred as 3.4Ag/Ti) and 6.4 mg Ag₂O/g TiO₂ (referred as 6.4Ag/Ti). The Ag content was determined by titration of the remainder Ag⁺ in the supernatant liquor and corroborated from the XRD patterns with the determination of the areas of the silver peaks (see Figure 1).

A commercial titania (Aldrich, TiO₂ 99 % anatase, referred as CA) was also employed to compare with the materials synthesized in the laboratory.

Methylene blue (MB, cationic, Biopack for microscopy, 99%) was chosen as adsorbate. MB is a basic blue dyestuff, classification number 52015, λ_{\max} = 664 nm, M_w = 373.9 g mol⁻¹. For aqueous dye solution only double distilled water was used. Solution pH was kept constant and equal to 8 by using a phosphate buffer (Na₂HPO₄/NaH₂PO₄).

Nitrogen adsorption isotherms

The nitrogen adsorption isotherms at 77.6 K were measured with a Micrometrics Model Accelerated Surface Area and Porosimetry System (ASAP) 2020 instrument. Each sample was degassed at 373 K for 720 min at pressure of 10⁻⁴ Pa.

Transmission electron microscopy

Transmission electron microscopy was performed using a JEOL 100 CX transmission electron microscope, operated at 100 kV with magnification of 100.000 X. Observations were made in a bright field. Powdered samples were placed on copper supports of 2000 mesh.

X-ray powder diffraction

Powder ray diffraction (XRD) data were collected via a Philips PW 1710 diffractometer with Cu K_α radiation (λ = 1.5418 Å) and graphite monochromator operated at 45 kV; 30 mA and 25 °C.

Scanning electron microscopy

Scanning electron microscopy was performed using a JEOL 35 CF (Japan 1983) scanning electron microscope.

Solid state conductivity measurements

Solid State Conductivity (SSC) measurements were performed by means of ac impedance spectroscopy with an Agilent 4284A LCR meter in the frequency range of 20Hz-1MHz in a close environment with Silica gel desiccant, between 70-290°C.

The powdered sample was pressed to form a pellet (diameter: 12 mm; thickness: 1.0-1.4 mm). Cu electrodes were attached to both sides of the pellets by silver paint. The samples were kept for at least 30 minutes at each temperature so they could stabilize before the ac impedance measurements were carried out.

The impedance data were represented in a Nyquist plot, in which the imaginary component of impedance ($\text{Im}(Z)$, in Ohm) is represented against the real part of it ($\text{Re}(Z)$). [10].

To determine the conductivity at each temperature the following relationship is used:

$$\sigma = (l/A).(1/R) \quad (1)$$

where (l/A) is the cell constant (l = width, A = geometric area) and R is the resistance obtained from the intersection of the impedance curve with the real axis in the complex plane when the frequency trends to zero.

Photodegradation

To evaluate the photocatalytic activity of the different adsorbents the degradation of MB was used. This dye is commonly used as standard target in this kind of tests. Real effluents are composed by a mixture of dyes and other components, but we employed pure MB solutions with buffer to avoid interferences and other effects which may difficult the interpretation results. Since degradation efficiency is inversely affected by the dye concentration [11], the highest concentration possible to obtain the maximum experiment time was used ($C = 0.036$ mM) under UV irradiation at 25 °C. The UV light was supplied by a DESAGA UV 131000 lamp ($\lambda = 366$ nm). Light intensity was estimated as $I_a = 2, 7 \times 10^{-6}$ mol photon s^{-1} from data given by the supplier. Samples were made with 0.2 g of catalytic material immersed in 10 mL of dye solution.

Dye adsorption experiments

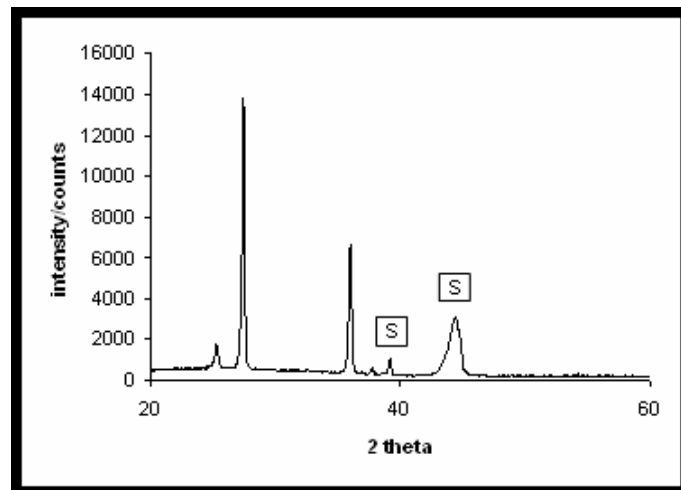
Dye adsorption test was performed by immersion of 50 mg of each adsorbent in 5 mL of dye solution. The range of concentration was (0.00432-0.036) mM. The flasks were then shaken for the different adsorption times at 25, 35, and 45 °C. At the end of the adsorption period the supernatant was centrifuged for 5 min at a speed of 3500 min^{-1} . The supernatant MB concentration before and after adsorption was determined using a Spectronic 20 UV-VIS spectrophotometer at 664 nm respectively.

Results

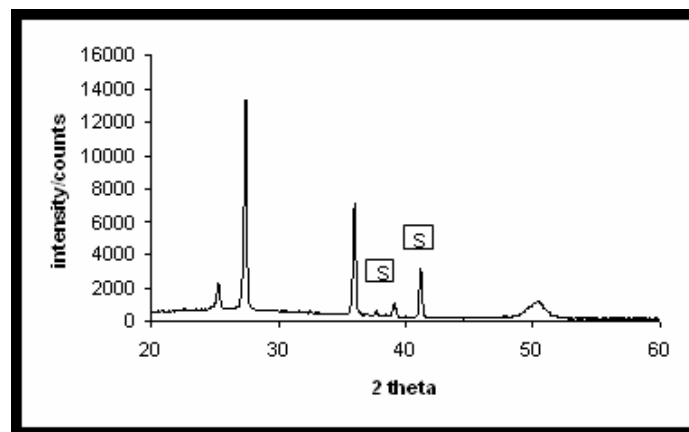
Materials Characterization

XRD diffraction

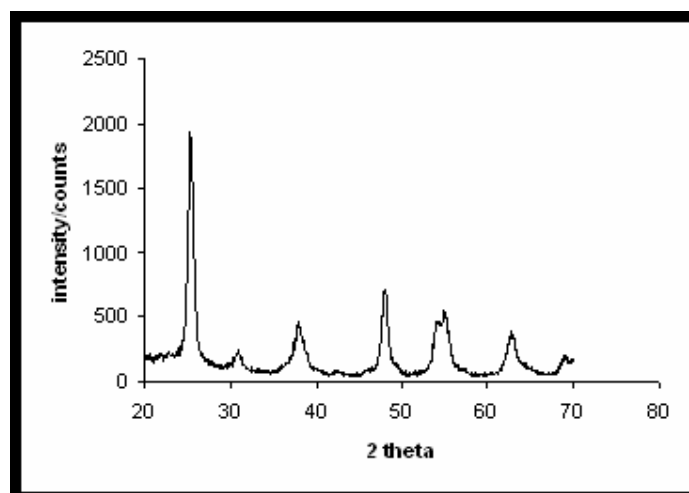
The XRD pattern (Figure 1) for AST indicates that main peaks were attributed to TiO_2 in the crystalline forms anatase and rutile [12]. Peaks related with silver in 3.4Ag/Ti and 6.4Ag/Ti are indicated by S on the graphs [12, 13]. The sharpness of peaks indicates the existence of nanocrystalline titania [14]. With Ag addition the material augmented their crystallinity, as demonstrated by the increased sharpness of peaks.



(A)



(B)



(C)

Figure 1. XRD patterns of: A) 3.4Ag/Ti ; B) 6.4Ag/Ti; C) AST. S denotes the silver peaks.

The composition of the different synthesized titanias was determined by using the XRD patterns and the correlations giving by Zhang and Banfield [15]. The weight fraction of rutile (W_R), anatase (W_A) and brookite (W_B) in the sample was determined with the relationships:

$$W_A = \frac{k_A A_A}{k_A A_A + A_R + A_B A_B} \quad (2)$$

$$W_R = \frac{A_R}{k_A A_A + A_R + A_B A_B} \quad (3)$$

$$W_B = \frac{k_B A_B}{k_A A_A + A_R + A_B A_B} \quad (4)$$

where A_A , A_B and A_R are the integrated intensity of the anatase (121, $2\theta = 25.44^\circ$), brookite (101, $2\theta = 30.98^\circ$) and rutile (111, $2\theta = 27.54^\circ$) respectively, obtained from the XRD patterns by deconvolution using the PeakFit program. The coefficients $k_A = 0.886$ and $k_B = 2.721$ were obtained from reference [15].

The composition of the different samples were AST ($W_A = 0.818$, $W_B = 0$, $W_R = 0.182$), 3.4AgTi ($W_A = 0.027$, $W_B = 0.973$, $W_R = 0$), 6.4AgTi ($W_A = 0.035$, $W_B = 0.965$, $W_R = 0$). Then, the AST composition was altered by the inclusion of Ag, while the different materials doped with Ag had almost the same composition of the titania matrix. Moreover, the addition of silver modified the titania composition. Anatase content was reduced and rutile disappeared, whilst brookite appeared as the main component.

SEM studies

Figures 2 and 3 show SEM micrographies of the studied materials. The SEM study revealed that the microscopic morphology of CA is less compact than that of AST. The addition of Ag causes a change in the microscopic titania structure, that becomes more open. The change increases with increased silver content. It was previously informed that Ag doping affects the TiO_2 structure [16], which is also consistent with the change in composition. The Ag(I) ion is considerably larger than the Ti(IV) ion (0.126 nm as opposed to 0.067 nm) [17]. Thus, the Ag(I) does not easily fit into the titania crystal lattice. As a result, the Ag(I) ion is expected to be primarily found in the grain boundary layers, which is consistent with the observation that the local concentration of Ag were found to be higher in the more porous regions and lower in the denser regions [16]. The structure was not compacted at this level of amplification because Ag was incorporated after calcination [16].

TEM analysis

Figures 1 and 2 in the supplementary material (SM) show the TEM microphotographs of the studied materials. CA shows relatively large granules (about 100 nm diameter) without any particular structure. The AST material shows a much more fine structure, formed by agglomerations of small platelets (between 5 and 14 nm diameter). The addition of Ag causes an increase in the size of platelets which become polydisperse. The size of platelets increases with increasing Ag content (Figure 2 in SM). This indicates that the structure was modified and probably compacted at this level of amplification (i.e., mesoscopic), although Ag was incorporated after calcination even

though the condition proposed by Li et al. [16] to produce compaction is the incorporation of Ag before calcination.

As a conclusion, the incorporation of Ag causes the macroscopic structure to be more open, whilst at a nanoscopic scale the structure is more compact.

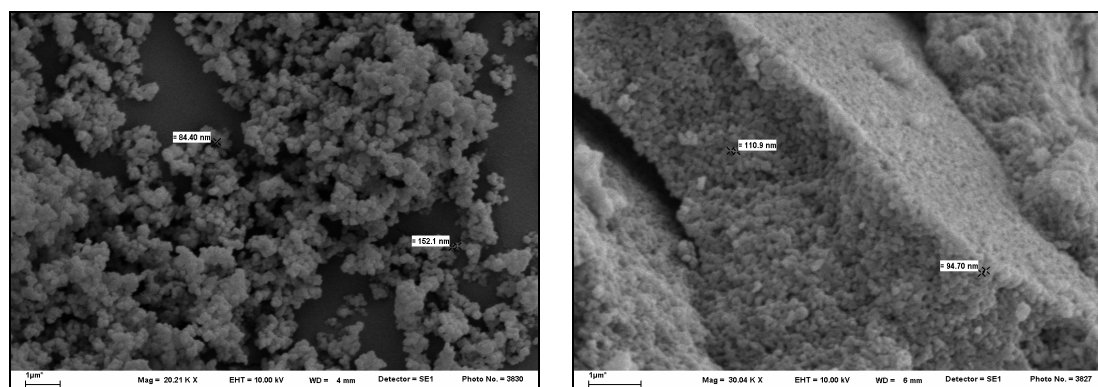


Figure 2. SEM images of AST TiO₂ (right) and CA (left).

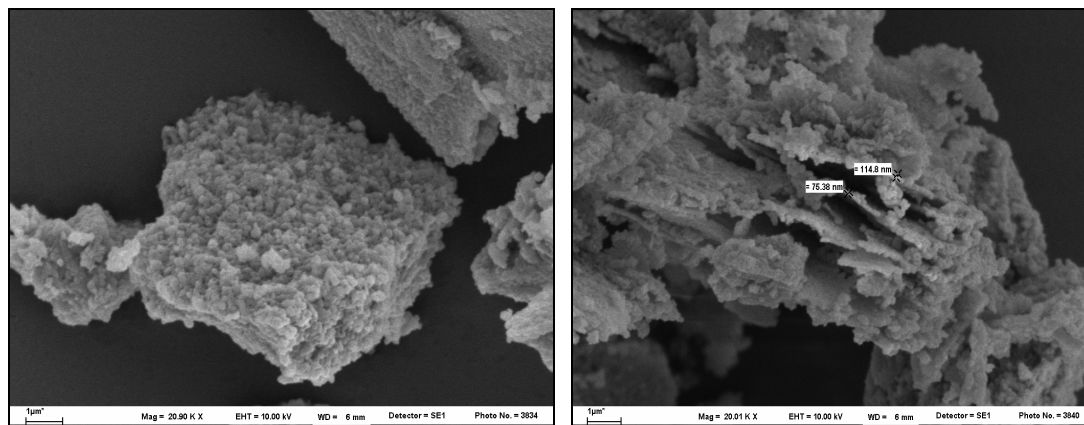


Figure 3. SEM microphotographs of 3.4Ag/Ti (left) and 6.4Ag/Ti (right).

Nitrogen adsorption analysis

The N₂ adsorption isotherm (Figure 3 in SM) indicates that 6.4Ag/Ti shows the typical type III isotherm. The 3.4Ag/Ti and AST materials isotherms are of the same kind. Isotherms of this type are not common but the adsorbate-adsorbent interactions play an important role. The type *H*₃ loop, which does not exhibit any limiting adsorption at high p/p^0 , is observed with aggregates of plate –

like particles giving rise to slit-shaped pores [18]. This finding is consistent with the SEM and TEM results.

Figure 4 in SM shows the t -plot for 6.4Ag/Ti. The 3.4Ag/Ti and AST t -plots are similar. This kind of plot is also compatible with slit-shaped pores [19, 20].

Figure 4 shows the distribution of pore radii for the three adsorbents. The pores of the three materials are of the size considered as mesopores by IUPAC (Pore radius between 1-25 nm), but the 6.4Ag/Ti material has some proportion of macropores (radius > 25 nm).

The adsorption results are summarized in Table 1. As previously determined [21], the specific area for AST was 35 m²/g. When Ag is incorporated to titania the value is lower, between 5 and 9 m²/g because some mesopores of TiO₂ are filled or closed by Ag⁺ ions [12]. The Ag(I) radius (0.126 nm) is small enough to allow the inclusion of silver ions in the smaller mesopores. However, an increase in the Ag content produces an increase in specific area, probably caused by separation of platelets. This is evidenced by an increase in the adsorption average pore diameter determined by BET and the increase in the cumulative pore volume.

Table 1. Nitrogen adsorption data of the synthesized adsorbents. A_{sp} : single point surface area at $P/P_0=0.2002$, A_{BET} : BET surface area, A_{text} : t -plot external surface area, A_{BJHac} : BJH adsorption cumulative surface area of pores between 3.4 and 600 nm diameter, A_{BJHdc} : desorption cumulative surface area of pores between 3.4 and 600 nm diameter, D_{aap} : adsorption average pore diameter by BET (4V/A), D_{aBJH} : BJH adsorption average pore diameter, D_{dBJH} : BJH desorption average pore diameter, V_{spat} : single point adsorption total pore volume of pores, $V_{BJHacvp}$: BJH adsorption cumulative volume of pores, $V_{BJHdcvp}$: desorption cumulative volume of pores.

Sample	A_{sp} (m ² /g)	A_{BET} (m ² /g)	A_{text} (m ² /g)	A_{BJHac} (m ² /g)	A_{BJHdc} (m ² /g)	D_{aap} (Å)	D_{aBJH} (Å)	D_{dBJH} (Å)	V_{spat} (cm ³ /g)	$V_{BJHacvp}$ (cm ³ /g)	$V_{BJHdcvp}$ (cm ³ /g)
3.4Ag/Ti	4.9962	5.1720	6.2155	5.235	8.4792	252.40	318.79	199.23	0.0326	0.0417	0.0422
6.4Ag/Ti	8.0859	8.600	11.957	7.400	10.373	202.87	268.03	194.09	0.0436	0.0495	0.0503
AST	30.58	34.9	55.60	16.69	39.80	17.59	33.40	16.87	0.0153	0.0164	0.0168
CA	3.515	3.884	6.179	2.001	2.923		191.8	135.1	0.00899	0.0096	0.0099

The linear part of the t -plot corresponds to the adsorption before pore filling [19, 20]. The fitting of these points by Langmuir and Freundlich isotherms give some insight about the surface properties of adsorbents. It is interesting that the fitting for 3.4Ag/Ti material is better when Freundlich isotherm is used ($R^2 = 0.9920$) than when Langmuir equation is used ($R^2 = 0.9797$); whereas this situation is inverse for the 6.4Ag/Ti material (Freundlich $R^2 = 0.9813$, Langmuir $R^2 = 0.9904$). Since Langmuir equation is associated with homogeneous adsorbent surfaces, and Freundlich isotherm with heterogeneous ones [22], it may be concluded that the low Ag content material exposes to adsorption a predominantly heterogeneous surface (TiO₂ + Ag₂O), while the separation of platelets by and increasing Ag inclusion exposes more TiO₂ surfaces thus reducing the proportion of Ag₂O in the total specific area.

In conclusion, the synthesis of titania by using Ti isopropoxide gives a lamellar mesoporous material composed by small anatase and rutile platelets. The inclusion of Ag increases the

crystallinity of the titania matrix and the size of mesoplatelets and changes the composition to predominantly brookite with some anatase, without rutile. At low silver content, Ag(I) probably fills the mesopores giving a decrease in the total specific area. Increasing the Ag content, its inclusion in the grain boundary layers causes an increase in the separation between platelets.

Solid state conductivity measurements

Nyquist diagrams at 120 °C are shown in Figure 5. In order to a better clarity, 10^6 was added to the data for AST and 5×10^5 to those of 3.4Ag/Ti materials. From these diagrams the electrical resistance for each composition was determined using as a model of the equivalent circuit of the system a simple RC parallel circuit with a specific software (B.A. Boukamp Equivalent Circuit version 3.97). From these resistances the conductivity at each temperature was determined and plotted against T^{-1} in Figure 6 according the equation:

$$\sigma = \frac{\sigma_0}{T} \exp(-E_a/kT) \quad (5)$$

At low temperature (LT, $T < 100$ °C) the conductivity of all samples is almost similar. Increasing the temperature (100 °C $< T < 200$ °C, medium temperature region, MT), σ strongly decreases. The two preceding regions are not reversible on cooling. At high temperature (HT, $T > 200$ °C) σ increases. The 6.4Ag/Ti sample shows conductivity about half magnitude order higher than the 3.4Ag/Ti sample, and one order of magnitude higher than that of the AST material.

The interpretation of results is that below 100 °C the conductivity is affected by the presence of water, since the samples were not thermally treated previously. The decrease in σ in the MT region may be attributed to sample dehydration, and above 200 °C the conductivity increase may be attributed to Ag^+ contribution as charge carrier.

The analysis of the HT results with Equation 5 gave the data of Table 2. As it can be seen in this table, the value of σ_0 for AST is much smaller than that of the Ag-doped materials, reflecting the relevant contribution of silver ions to the conductivity.

The activation energy for the conductivity is also higher for Ag-doped materials than for the AST sample, although the difference is not statistically significant. In fact, the three E_a confidence intervals are superimposed. The average value for the silver doped samples is $E_a = 23.2 \pm 3.3$ kJ.mol⁻¹. Assuming that the difference in E_a between AST and Ag/Ti materials is significant, the higher value for the latter may reflect the difficulty of move the Ag^+ ions (bigger than the Ti^{4+} ones) through the TiO_2 matrix.

Work is in progress to clarify these suppositions.

Table 2. Analysis of the conductivity dependence of solid adsorbents on temperature and composition. Errors were computed with a significance level of 0.90.

Material	σ_0 (S cm ⁻¹)	E_a (kJmol ⁻¹)
AST	0.0049 ± 0.0038	11.8 ± 10.6
3.4Ag/Ti	2.24 ± 7.64	21.9 ± 5.1
6.4Ag/Ti	15.9 ± 13.8	24.2 ± 4.3

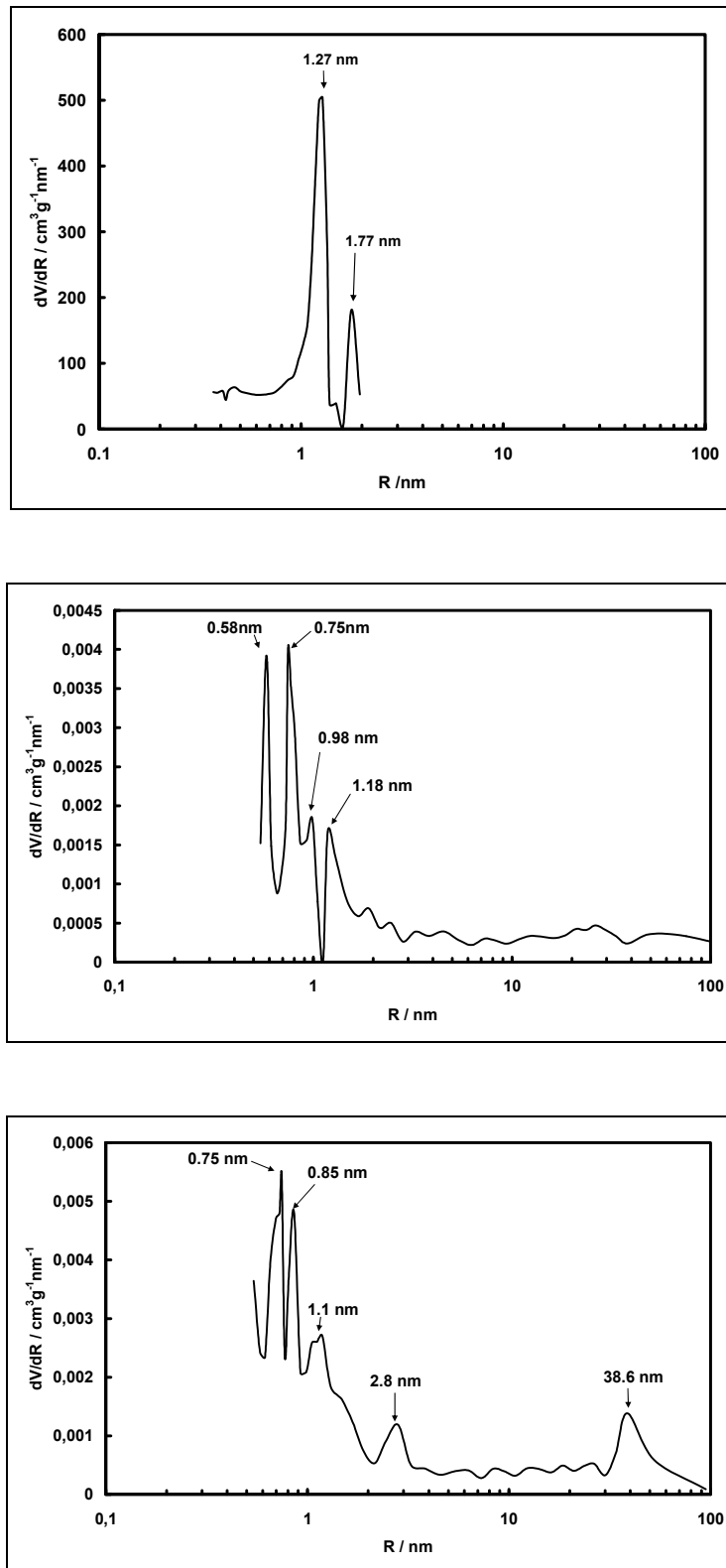


Figure 4. dV/dR vs. R plot for AST. (above), 3.4Ag/Ti (middle) and 6.4Ag/Ti (below).

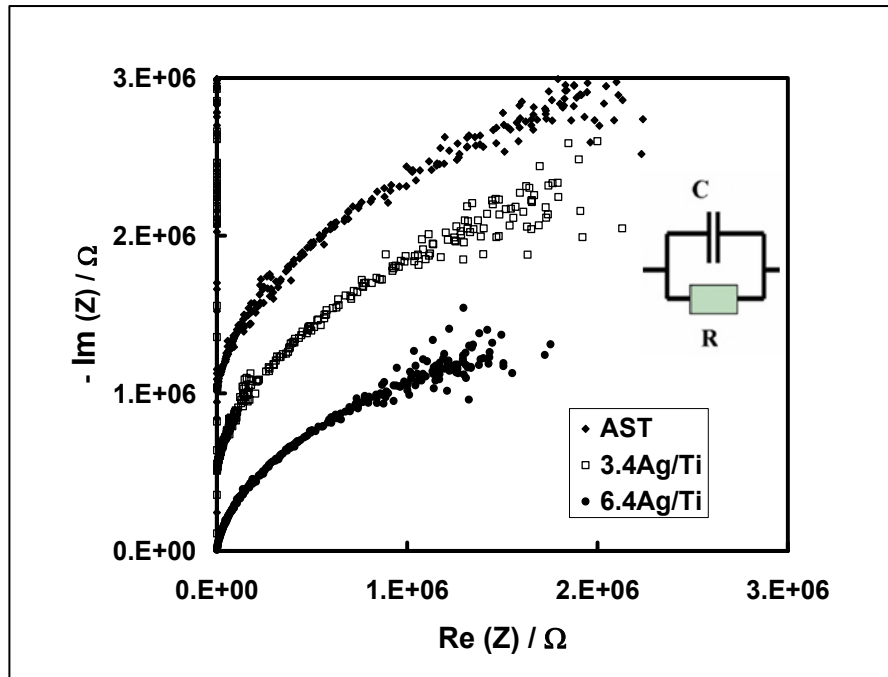


Figure 5. Nyquist diagram at 120 °C. ♦ : AST + 10^6 ; □ : 3.4Ag/Ti + 5×10^5 ; • : 6.4Ag/Ti.

Dye adsorption results

Two isotherms equations are used in this work to analyze the MB adsorption on the different adsorbents. One is the Langmuir equation, based on the hypothesis that the maximum adsorption corresponds to a saturated monolayer of adsorbate molecules on the adsorbent surface, with constant energy of interaction:

$$q_e = \frac{q_{mon} K_L C_e}{1 + K_L C_e} \quad (6)$$

where K_L is the Langmuir constant related to the energy of adsorption, C_e is the total concentration of dye in solution, q_e is the amount of dye (mmol) adsorbed per gram of adsorbent and q_{mon} (mmol/g of adsorbent) is the maximum amount of adsorption corresponding to complete coverage on the surface by a monolayer of dye.

The other isotherm is the Freundlich one, which can be used for non-ideal sorption that involves heterogeneous adsorbent surfaces and is expressed by the equation:

$$q_e = K_F C_e^{1/n_F} \quad (7)$$

where K_F is related with the adsorption capacity and $1/n_F$ is related with the adsorption intensity. In general, as K_F increases the adsorption capacity of an adsorbent for a given adsorbate augments, and it can be related to the surface energy as $K_F = RTn_F e^{\Delta H/RT}$. The magnitude of the exponent $1/n_F$ gives an indicator of how favorable is the adsorption [23].

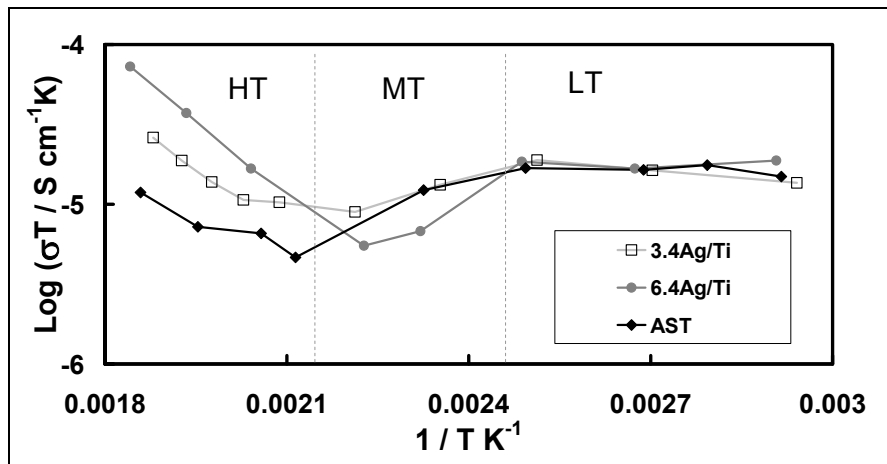


Figure 6. Representation of equation (2) for the three titania samples.

Results of the application of both equations are summarized in table 1 in SM. In general, both isotherms fit the MB adsorption data with almost the same correlation coefficients for all the adsorbents, including commercial anatase and the untreated titania (AST). There is not assurance that the derivation of the Freundlich equation is unique; consequently, if the data fit the equation, it is only likely, but not proved, that the surface is heterogeneous [22]. Since in many cases the Langmuir equation gives adequate results in systems in which surface heterogeneity is known to be present [24] the fitting of the data by both models with similar correlation coefficients is possible.

Figure 7 shows the value of $1/n_F$ for the adsorption on the different adsorbents. It may be seen that the adsorption intensity on CA and 3.4Ag/Ti monotonically decreases when T increases, while there is a maximum at 35 °C for AST and 6.4Ag/Ti. Since it is expectable that physical adsorption decrease as the temperature rises, the above behavior for AST and 6.4Ag/Ti may mean that there is a change in the nature of adsorption when passing from the 25 to 35 °C interval to the 35 to 45 °C temperature range. Notice that this occurs in AST and 6.4Ag/Ti, which are the two adsorbents with higher specific surface and with higher proportion of titania at the surface. This may mean that in these two latter adsorbents, the adsorption is at least partially of chemical nature at low temperature and mainly of physical nature at high temperature. As it can be seen in Figure 7, 3.4Ag/Ti material shows an intermediate behavior: although $1/n_F$ decreases with increasing temperature, this decrease is not so pronounced as that seen in the CA material. Another observation is that the adsorption intensity is in general higher in Ag-doped materials than in the pure titania ones.

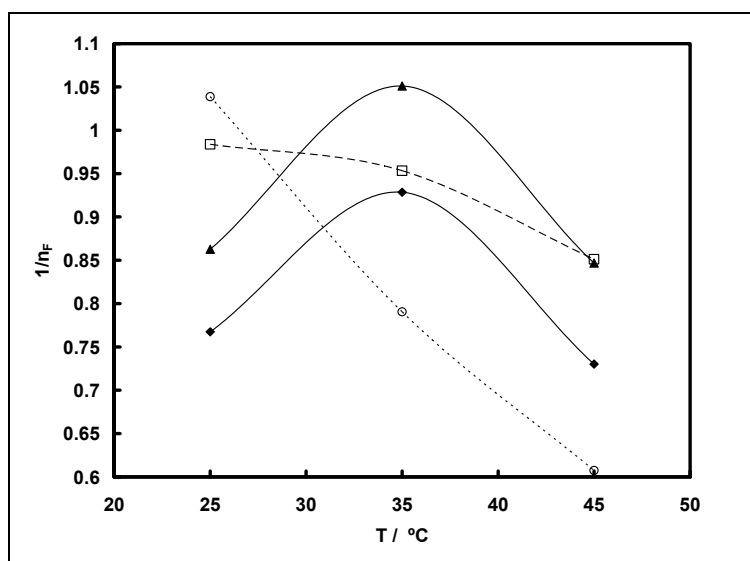


Figure 7. Intensity of adsorption for MB on different adsorbents as a function of temperature. ○: CA; ◆: AST; □: 3.4Ag/Ti and ▲: 6.4Ag/Ti.

Adsorption kinetics

Figure 8 shows as examples the adsorbed amount as a function of time for both Ag – doped materials for one of the total dye concentration used. The first stages of the adsorption kinetics of MB on Ag doped titania followed the Lagergren first order rate model [25]:

$$\ln (q_{eq} - q_t) = \ln q_{eq} - k_{ads} \cdot t \quad (8)$$

where q_{eq} and q_t are the amount of dye adsorbed per unit mass of the adsorbent (in $\text{mmol} \cdot \text{g}^{-1}$) at equilibrium time and time t , respectively, and k_{ads} is the rate constant. The values of k_{ads} at three different temperatures (25, 35 and 45 °C) were independent of the initial concentration (C_0) of dye. The average values for the two Ag doped titanias and the three temperatures are given in Table 3. It may be seen that the rate of adsorption diminished with the increase of temperature in both adsorbents.

Table 3. The values of the kinetic first order constant k_{ads} (h^{-1}) for MB adsorption on silver-treated titania.

Adsorbent	25°C	35°C	45°C
3.4Ag/Ti	0.060 ± 0.002	0.0484 ± 0.0009	0.043 ± 0.002
6.4Ag/Ti	0.1127 ± 0.0006	0.00050 ± 0.00001	0.00123 ± 0.00001

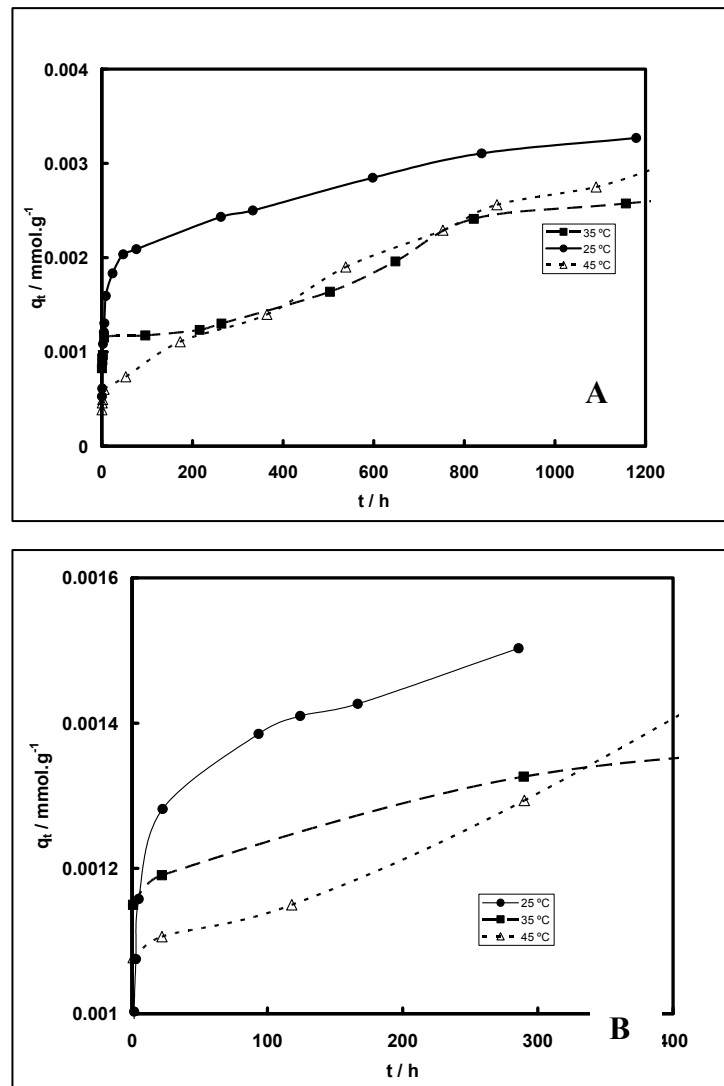


Figure 8, Adsorption kinetics of MB on (A): 3.4Ag/Ti, $C_0 = 0.036 \text{ mmol.L}^{-1}$, (B): 6.4Ag/Ti, $C_0 = 0.036 \text{ mmol.L}^{-1}$.

Photodegradation properties

Figure 9 shows the degradation of MB on diverse adsorbents: Ag/TiO₂, AST, and CA. The negative time in Figure 9 is the period in which the TiO₂ materials were mixed with dyes in darkness. The positive time is that in which the mixture is exposed under UV light [26]. The behavior of a MB solution without adding any catalyst was also plotted for comparison.

The commercial anatase (CA) was more efficient than the synthesized materials (with and without Ag). The less efficient was AST, and efficiency increased with increasing Ag content. The maximum degradation with CA was 98.72 % and was reached in 3 hours. For 6.4Ag/Ti the maximum was 96.96 % obtained at 4.92 hours. The maximum for 3.4Ag/Ti was 95.82 % reached at

5.5 hours, while for AST was 95 % attained in 8.58 hours. To compare the speed of degradation, the time in which 90 % of degradation was reached was taken. Results were: CA: 1 h, 6.4Ag/Ti: 2.1 h, 3.4Ag/Ti: 3.2 h and AST: 5.4 h. The efficiency was similar to that of Ag-doped titania films in literature [7]. The efficiency (per gram of adsorbent) was strongly dependent on the size of grains of the catalyst. The data in Figure 9 were obtained in finely powdered material. Coarsely granulated catalysts showed efficiency (per gram of adsorbent) which depended on the granules' size. However, when computed on the basis of the adsorbent area, results were similar to those of Figure 9.

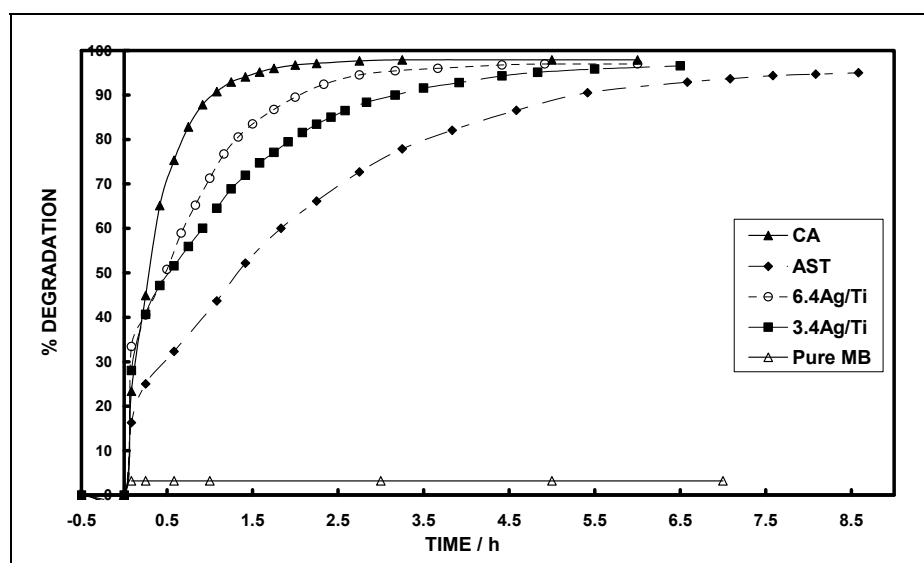


Figure 9. MB degradation for different TiO_2 materials. \blacktriangle : CA; \blacklozenge : AST; \blacksquare : 3.4Ag/Ti; \circ : 6.4Ag/Ti; \triangle : methylene blue without catalyst addition.

The specific surface of the precursor is higher than that of the Ag-doped materials, but, considering that the MB degradation occurs at the surface of the catalyst, the inclusion of Ag has improved the efficiency of the catalyst surface. The effect in powdered Ag-doped titania is different to that observed in titania films, in which the inclusion of more than 4 % Ag produced a reduction in the overall catalytic efficiency, while a minor content has the reverse effect [7]. Probably the excess of Ag in those films migrates to the interior of the titania matrix and becomes inaccessible to the dye molecules.

The degradation follows a first order kinetics with the equation

$$\ln C_t = -k_{\text{deg}}t + \ln C_0 \quad (9)$$

where C_0 is the initial concentration of dye, C_t that at time t , and k_{deg} the kinetic constant. The data deviate from the straight line when the degradation reaches about 90 %. Table 4 shows the values of k_{deg} for the four adsorbents. It may be seen that the faster degradation is shown by the CA catalyst,

followed by the silver - doped materials decreasing with decreasing Ag content. The lower kinetic constant is that of AST material.

Table 4. First order degradation kinetic constant.

Adsorbent	CA	AST	3.4 Ag/Ti	6.4 Ag/Ti
$k_{\text{deg}} / \text{h}$	0.207±0.015	0.0161±0.0034	0.0929±0.0099	0.103±0.055

Conclusions

Material characterization

AST was composed by crystals of anatase and rutile. The inclusion of Ag in this material changes the composition to anatase and brookite and modifies its structure which becomes more open at a microscopic level when Ag content increases as seen by SEM. However, at the same time there is some reduction in porosity at a mesoscopic level. This was attributed to the inclusion of Ag(I) in the grain borders, because its radius is larger than Ti(IV) one. When observed by TEM, CA shows relatively large granules (about 100 nm diameter) without any particular structure. The AST material shows a much more fine structure, formed by agglomerations of small platelets (between 5 and 14 nm diameter). The addition of Ag causes an increase in the size of platelets which become polydisperse. The size of platelets increases with increasing Ag content. Nitrogen adsorption analysis of AST and Ag doped titanias shows isotherms and t -plots which are compatible with mesoporous materials having slit-shaped pores as observed in aggregates of plate-like particles. The specific area of AST was higher than that of Ag doped materials, because Ag is probably included inside micropores or obstructs them. However, an increase in Ag content increases the average pore diameter and specific area of the material, probably by inclusion of Ag ions between platelets increasing their separation. Langmuir equation fits best than that of Freundlich the adsorption of nitrogen on AST and 6.4Ag/Ti materials, while the inverse is observed in 3.4Ag/Ti. This means that the surface of 3.4Ag/Ti is more heterogeneous than that of 6.4Ag/Ti material, which seems paradoxical. The explanation is that an increase in Ag content causes separation between platelets then exposing more TiO₂ surface to adsorption. This increases the proportion of TiO₂ to Ag₂O exposed to adsorption.

Conductivity experiments on solid materials showed that the value of σ_0 for AST is much smaller than that of the Ag-doped materials, reflecting the relevant contribution of silver ions to the conductivity. The activation energy for the conductivity is also higher for Ag-doped materials than for the AST sample. The average value for the silver doped samples is $E_a = 23.2 \pm 3.3 \text{ kJ.mol}^{-1}$. Assuming that the difference in E_a between AST and Ag/Ti materials is significant, the higher value for the latter may reflect the difficulty of move the Ag⁺ ions (bigger than the Ti⁴⁺ ones) through the TiO₂ matrix.

MB adsorption and degradation

The experimental data for all the tested adsorbents fit both the Langmuir and the Freundlich isotherms. Although not very common, this is a possible situation, in which Langmuir isotherm fits well to an adsorption on a heterogeneous surface. The adsorption intensity on CA and 3.4Ag/Ti monotonically decreases when T increases, but there is a maximum at 35 °C for AST and 6.4Ag/Ti. The behavior of 3.4Ag/Ti material was intermediate. This may mean that in these adsorbents, the adsorption is at least partially of chemical nature at low temperature and mainly of physical nature

at high temperature. Another observation is that the adsorption intensity is in general higher in Ag-doped materials than in pure titania.

The initial adsorption kinetics follows the Lagergren first order rate model. The values of k_{ads} at three different temperatures (25, 35 and 45 °C) were independent on the initial concentration (C_0) of dye. The rate of adsorption diminished with the increase of temperature in both adsorbents. This is expectable in physical adsorption.

Photodegradation of MB on AST and Ag-doped materials was 96 % in less than 6 hours, showing efficiency similar to other Ag-doped materials in literature. However, CA was more efficient. The degradation capacity per gram of adsorbent is higher for AST, but that for surface unit of photocatalyst is higher for Ag-doped titanias. The degradation kinetics followed a first order equation.

Acknowledgements. This work was supported by a grant of the Universidad Nacional del Sur. PVM and MF are adjunct researchers of the Consejo Nacional de Investigaciones Científicas y Técnicas (CONICET) de la República Argentina. CEZ has a fellowship of CONICET.

References

- [1] Y. Yan, X. Qiu, H. Wang, L. Li, X. Fu, L. Wu, G. Li. *J. Alloys Compd.*, **2008**, 160 (1-2), 491.
- [2] G. Strukul, R. Gavaguin, F. Pinna, E. Modafferri, S. Perathoner, G. Centi, M. Marella, M. Tomaselli, *Catal. Today*, **2000**, 55, 139.
- [3] S. Castillo, T. López, *Appl. Catal. B: Environ.*, **1998**, 15, 203.
- [4] T. López, R. Gómez, G. Pecci, P. Reyes, X. Bokhimi, O. Novaro, *Mater. Lett.*, **1999**, 40, 59.
- [5] J. Matsuoka, R. Naruse, H. Nasu, K. Kamiya, *J. Non Cryst. Solids*, **1997**, 218, 151.
- [6] W.D. Kingedry, H.K Bowen, D.R Uhlman. *Introduction to Ceramics*; 2nd Ed., Wiley, New York, 1976, p. 457.
- [7] C. He, Y. Yu, X. Hu, A. Larbot. *Applied Surf. Sci.*, **2002**, 200, 239.
- [8] C.C. Chang, J. Y. Chen, T.L. Hsu, C.K. Lin, C.C. Chan, *Solid Films*, **2008**, 516, 1743.
- [9] D. Reyes Coronado, G.R. Gattorno, M.E. Espinosa Pesqueira, C. Cab, R. de Coss, and G. Oskam, *Nanotechnology*, **2008**, 19, 145605.
- [10] R. Mcdonald. *J. Impedance Spectroscopy. Emphasizing Solid Materials and Systems*. Wiley & Sons, Chap.1, 1987, p. 16.
- [11] C.C Chen, C.S. Lu, Y.C. Chung, J.L. Jan, *J. Hazardous Mat.*, **2006**, 141, 520.
- [12] H.W. Wang, H.C. Lin, C.H. Kuo, Y.L. Cheng, Y.C. Yeh, *J. Phys. Chem. Solids*, **2008**, 69, 633.
- [13] H. Ortiz-Ibarra, N. Casillas, V. Soto, M. Barcena-Soto, R. Torres-Vitela, W. de la Cruz, S. Gómez-Salazar, *J. Colloid Interface Sci.*, **2008**, 314, 562
- [14] C.C. Chang, C.K. Lin, C.S. Hsu, C.Y. Chen, *Thin Solid Films*, **2006**, 494, 274.
- [15] H. Zhuang, J.F. Banfield, *J. Phys. Chem. B*, **2000**, 3481.
- [16] X.S. Li, G.E. Fryxell, C. Wang, M.H. Engelhard, *Microporous Mesoporous Mat.*, **2008**, 111, 639.
- [17] F.H. Speeding, K. Gschneider, in *CRC Handbook of Chemistry and Physics*, 53 Ed. CRC Press, Cleveland, Ohio, 1972, p. F-17.
- [18] K.S.W. Sing, Everett, R.A.W. Haul, L. Moscou, R.A. Pierotti, J. Rouquérol, T. Siemieniewska, *Pure & Appl. Chem.*, **1985**, 57(4), 603.
- [19] F. Radjy, E. J. Sellevold, *J. Colloid Interface Sci.*, **1972**, 39(2), 367.

- [20] E.J. Sellevold, F. Radjy, *J. Colloid Interface Sci.*, **1972**, 39(2), 379.
- [21] C. Zubieta, P. Messina, C. Luengo, M. Dennehy, O. Pieroni, P. Schulz, *J. Hazardous Materials*, **2008**, 152, 765.
- [22] A.W. Adamson, A.P. Gast, *Physical Chemistry of Surfaces*, 6th ed., Wiley, New York, (1998), pp. 393–394.
- [23] E. Erdem, G. Colgeçen, R. Donat, *J. Colloid Interface Sci.*, **2005**, 282, 314.
- [24] P. C. Hemenz, R. Rajagopalan, *Principles of Colloid and Surface Chemistry*, Dekker, New York, 3rd ed., 1997, pp. 336-338.
- [25] S. Wang, Z. H. Zhu, A. Coomes, F. Haghceresht, G.Q. Lu, *J. Colloid Interface Sci.*, **2005**, 284,440.
- [26] A. Syoufian; K. Nakashima. *J. Colloid Interface Sci.*, **2008**, 317 (2), 507.